International Journal of Applied Mathematics
Volume 38 No. 12s, 2025
ISSN: 1311-1728 (printed version); ISSN: 1314-8060 (on-line version)

Thermal load reduction in buildings using transparent honeycomb insulation

Pawan Kumar Sharma, Jitendra Kumar, Anuj Baliyan*and Naresh Pant

Bareilly College, Bareilly, affiliated to MJPRU, Bareilly, Uttar Pradesh, 243001, India

pksharma1170@gmail.com, jitu14iitr@gmail.com,
anujbaliyan0405@gmail.com, pantnaresh411@gmail.com

Abstract

Improving the thermal performance of building envelopes is essential for reducing energy consumption and maintaining indoor thermal comfort across varying climatic conditions. This study presents an analytical and numerical investigation of thermal load reduction in buildings using opaque insulation and transparent insulation materials (TIM), with emphasis on polycarbonate honeycomb systems. A lumped heat balance-based thermal model is developed to account for conductive, convective, radiative, ventilation and solar heat transfer through walls, roofs, windows and doors. Simulations are carried out for a representative residential room located in three distinct Indian climatic zones: Leh (cold–dry), Bareilly (composite) and Hyderabad (warm–humid). Overall heat transfer coefficients (U-values) are evaluated for bare, opaque-insulated, and TIM-clad walls for insulation thicknesses ranging from 5 to 20 mm. The results show a consistent reduction in U-values with increasing insulation thickness, with opaque insulation providing the lowest values and TIM-clad walls offering a balanced combination of thermal resistance and solar transmission. Monthly analyses of solar irradiance, heat flux and thermal load indicate that insulation significantly reduces winter heat loss in cold climates and limits summer heat gain in warmer regions. A 20 mm insulation thickness is identified as optimal across all climates. The findings demonstrate the potential of transparent honeycomb insulation for energy-efficient and passive solar building applications.

Keywords: Honeycomb thermal insulation, Overall heat transfer coefficient, Solar intensity, Heat flux reduction, Building thermal performance

*Corresponding author

Received: December 11, 2025

International Journal of Applied Mathematics
Volume 38 No. 12s, 2025
ISSN: 1311-1728 (printed version); ISSN: 1314-8060 (on-line version)

Table 1: Nomenclature

Symbol	Description	Symbol	Description	Symbol	Description
U_L	Overall heat transfer coefficient	h_0	Outside convective heat transfer coefficient	K_b	Thermal conductivity of bare wall material
L_{wr}	Thickness of bare wall/roof	K	Thermal conductivity of concrete wall/roof	L_p	Thickness of plaster
K	Thermal conductivity	θ_r	Indoor air temperature	K_p	Thermal conductivity of plaster material
U_t	Total heat loss coefficient	L_j	Thickness of insulation	M	Mass of building component
L	Thickness of walls/roof	K_j	Thermal conductivity of insulation	C	Specific heat capacity of material
h_i	Inside convective heat transfer coefficient	L_b	Bare wall thickness	Q_{wl}	Periodic heat transfer through walls
$\frac{\partial\theta}{\partial t}$	Rate of change of temperature	Q_{wd}	Periodic heat transfer through window	Q_r	Periodic heat transfer through roof
Q_h	Heat flux by auxiliary heating source (heater effect)	Q_f	Heat transfer by furnishings inside room	Q_v	Heat loss/gain due to air ventilation and infiltration
Q_g	Heat conducted by underlying ground	β	Slat inclination angle	ε	Surface emissivity
S	Geometric shape factor	θ_s	Mean slat/glazing temperature	σ	Stefan–Boltzmann constant
Nu	Nusselt number	A	Aspect ratio	δ	Wall thickness
L	Cell width	r	Azimuth angle	d	Slat spacing

1 Introduction

The building sector in India accounts for a rapidly growing share of national energy demand required to maintain thermal comfort across diverse climatic zones through mechanical cooling and heating systems. With increasing urbanization, the demand for energy-efficient buildings has become a critical priority for sustainable development. Classical heat-transfer literature highlights that heat conduction through the building envelope, solar heat gains, and ventilation/infiltration collectively determine the dynamic cooling

Received: December 11, 2025

International Journal of Applied Mathematics
Volume 38 No. 12s, 2025
ISSN: 1311-1728 (printed version); ISSN: 1314-8060 (on-line version)

and heating load patterns experienced by buildings [1, 2]. Advanced simulation tools such as EnergyPlus, TRNSYS, ESP-r, and Design Builder enable detailed modelling of envelope components, material properties, occupancy dynamics, and HVAC system interactions [3, 4, 5, 6]. Building Information Modelling (BIM)-integrated workflows further enhance model accuracy by reducing geometric simplifications and improving thermal zoning assumptions [7, 8]. Several studies emphasize that simulation accuracy strongly depends on weather data inputs, solar radiation modelling, and internal heat-gain schedules [9]. Renewable energy technologies are not only a sustainable solution to the energy crisis but also represent a vital step toward a cleaner, healthier, and more secure future. By adopting alternative energy sources, long-term energy availability can be ensured while simultaneously protecting the environment. Simultaneously, thermal insulation provides a cost-effective and technically viable solution for reducing building energy consumption by minimizing heat transfer through the building envelope and lowering dependence on artificial heating and cooling systems. Solar heat-gain control, particularly through high-performance glazing and external shading devices, remains one of the most effective strategies, especially in hot climatic regions [10]. Phase change materials (PCMs) provide latent heat storage that shifts peak cooling loads and stabilizes indoor temperatures; however, challenges related to melting-point control and long-term thermal stability remain [11, 12]. Based on the above survey and for simulation purposes aimed at providing a comfortable indoor temperature of $\theta_r(t) = 297$ K in Leh, Bareilly, and Hyderabad, we consider a single room of a building with dimensions (15 ft × 18 ft × 12 ft). The sizes of the window and door are taken as (4 ft × 6 ft) and (3 ft × 7 ft), respectively.

2 Determination of fixed thermal resistance (R_{fixed})

Fixed thermal resistance of walls/roof in building is given by

$$\text{Fixed resistance } (R_{\text{fixed}}) = \text{Brick layer resistance } (R_{\text{brick}}) + \text{Plaster resistance } (R_{\text{plaster}}) \quad (1)$$

Where, $R_{\text{brick}} = \frac{L_b}{K_b}$ & $R_{\text{plaster}} = \frac{L_p}{K_p}$ are known as brick layer resistance and plaster resistance respectively. Let us consider that walls and roof of the building have been made by concrete materials. Expanded Polystyrene (EPS)/Polyurethane (PU) has been used as insulation. The thermal conductivity of brick masonry, cement plaster and insulation has been taken as 0.77 $\mathrm{W\,m^{-1}\,K^{-1}}$, 0.72 $\mathrm{W\,m^{-1}\,K^{-1}}$ and 0.04 $\mathrm{W\,m^{-1}\,K^{-1}}$ respectively. Polycarbonate honeycomb transparent insulation material has been used as TIM clad which have effective thermal conductivity for combined conductive and radiative effects varying from 0.18 $\mathrm{W\,m^{-1}\,K^{-1}}$ to 0.20 $\mathrm{W\,m^{-1}\,K^{-1}}$; but we have taken $K_{\text{TIM,eff}} = 0.18$ $\mathrm{W\,m^{-1}\,K^{-1}}$. Brick layer resistance and plastic resistance for cement plaster has been depicted in Table 2.

Table 2: Fixed thermal resistance (without insulation)

Layer	Thickness	Thermal conductivity ($\mathrm{W\,m^{-1}\,K^{-1}}$)	Thermal resistance ($\mathrm{m^2\,K\,W^{-1}}$)
Brick wall	9 inch	0.72	$R_{\text{brick}} = 0.319$
Cement plaster	0.02 m	1.00	$R_{\text{plaster}} = 0.02$

International Journal of Applied Mathematics
Volume 38 No. 12s, 2025
ISSN: 1311-1728 (printed version); ISSN: 1314-8060 (on-line version)

Therefore, fixed thermal resistance of wall/roof is given by

$$R_{\text{fixed}} = R_{\text{brick}} + R_{\text{plaster}} = 0.319 + 0.02 = 0.339 \text{ m}^2\,\text{K}\,\text{W}^{-1} \tag{2}$$

The value of R_{fixed} will be same for bare, opaque and TIM clad wall.

3 Determination of thermal conduction resistance (R_{cond})

Thermal conduction resistance (R_{cond}) of walls/roof is given by

$$R_{\text{cond}} = R_{\text{fixed}} + R_{\text{ins}} \tag{3}$$

For bare wall/roof, we have

$$R_{\text{ins}} = 0 \quad \text{and} \quad R_{\text{cond}} = R_{\text{fixed}} = \frac{L_b}{K_b} + \frac{L_p}{K_p} = 0.339 \text{ m}^2\,\text{K}\,\text{W}^{-1}.$$

Opaque insulation resistance (R_{ins}) for a wall/roof is given by

$$R_{\text{ins}} = \frac{\text{thickness of insulation}}{\text{thermal conductivity of insulation}} = \frac{L_j}{K_j} \tag{4}$$

For a wall with TIM clad, we have

$$R_{\text{ins}} = \frac{L_{\text{TIM}}}{K_{\text{TIM,eff}}} \tag{5}$$

Computed values of R_{cond} for opaque and TIM-clad walls have been given in Table 3, which shows that increasing insulation or TIM thickness from 5 to 20 mm leads to a continuous increase in both insulation resistance and overall conduction resistance for opaque and TIM-clad walls. For the same thickness, opaque insulation provides higher conduction resistance than TIM, indicating better heat transfer reduction. However, TIM-clad walls offer moderate thermal resistance while enabling solar transmission, making them suitable for passive solar applications.

Table 3: R_{cond} for opaque and TIM-clad wall

Opaque wall			TIM-clad wall		
Insulation thickness (mm)	R_{ins} ($\text{m}^2\,\text{K}\,\text{W}^{-1}$)	R_{cond} ($\text{m}^2\,\text{K}\,\text{W}^{-1}$)	**TIM thickness (mm)**	R_{ins} ($\text{m}^2\,\text{K}\,\text{W}^{-1}$)	R_{cond} ($\text{m}^2\,\text{K}\,\text{W}^{-1}$)
5	0.125	0.464	5	0.027	0.366
10	0.250	0.589	10	0.055	0.394
15	0.375	0.714	15	0.083	0.422
20	0.500	0.839	20	0.111	0.450

Received: December 11, 2025

International Journal of Applied Mathematics
Volume 38 No. 12s, 2025
ISSN: 1311-1728 (printed version); ISSN: 1314-8060 (on-line version)

4 Evaluation of overall heat transfer coefficient

We have assumed inside convective heat transfer coefficient (h_i) to be fixed at 8 $\mathrm{W\,m^{-2}\,K^{-1}}$ in each case of bare, opaque and clad with TIM, while outside convective heat transfer coefficient (h_0) vary as 10, 15, 20 and 25 $\mathrm{W\,m^{-2}\,K^{-1}}$ in all cases of 9 inches bare, opaque and clad with TIM. Formulae and computed values of overall heat transfer coefficient for bare, opaque and wall/roof clad with TIM are given in Table 4 and Table 5, respectively. Computational results as depicted in Table 5 conclude that the overall heat transfer coefficient decreases with an increase in the value of outdoor convective heat transfer coefficient. Therefore, the maximum value of 10 $\mathrm{W\,m^{-2}\,K^{-1}}$ for h_0 is preferable for optimization modelling of the insulation device for $h_i = 8$ $\mathrm{W\,m^{-2}\,K^{-1}}$.

Table 4: Formulation for overall heat transfer coefficient

Walls/roof	**Formula**
Bare	$\frac{1}{U_L} = \frac{1}{h_0} + \frac{L_{wr}}{K} + \frac{1}{h_i}$
Opaque walls/roof	$\frac{1}{U} = \frac{1}{h_i} + \sum_{j=1}^{n} \frac{L_j}{K_j} + \frac{1}{h_0}$
Wall/roof clad with TIM	$\frac{1}{U_{\mathrm{TIM}}} = \frac{1}{h_0} + \sum_{i} \frac{L_i}{K_i} + \frac{L_{\mathrm{TIM}}}{K_{\mathrm{TIM,eff}}} + \frac{1}{h_i}$

Table 5: Computed values of overall heat transfer coefficient ($\mathrm{W\,m^{-2}\,K^{-1}}$) for 9 inches wall

Walls/roof	**Insulation**	h_0 ($\mathrm{W\,m^{-2}\,K^{-1}}$)			
		10	15	20	25
Bare	Absent	3.03	2.51	1.96	1.45
Opaque walls/roof	5 mm	1.48	1.36	1.20	1.01
	10 mm	1.05	0.99	0.90	0.79
	15 mm	0.82	0.78	0.72	0.64
	20 mm	0.68	0.65	0.61	0.55
Wall/roof clad with TIM	5 mm	1.98	1.70	1.41	1.10
	10 mm	1.55	1.38	1.18	0.95
	15 mm	1.29	1.17	1.02	0.84
	20 mm	1.11	1.02	0.90	0.76

Continuing this process of computation for 4, 6, 9 and 14 inches wall thickness, we observe that the overall heat transfer coefficient decreases with an increase in wall thickness, as shown in Table 6. The computational results indicate that opaque insulated walls

Received: December 11, 2025

International Journal of Applied Mathematics
Volume 38 No. 12s, 2025
ISSN: 1311-1728 (printed version); ISSN: 1314-8060 (on-line version)

exhibit the lowest U-values, indicating the maximum reduction in heat transfer. Further, walls/roofs clad with TIM provide intermediate U-values, thereby offering a balance between thermal resistance and solar transmission, which is desirable for passive building applications. The geometrical interpretation for the variation of U with respect to wall thickness is illustrated in Fig. 1.

Table 6: Computed values of overall heat transfer coefficient ($\mathrm{W\,m^{-2}\,K^{-1}}$) for $h_0 = 10$ and $h_i = 8\ \mathrm{W\,m^{-2}\,K^{-1}}$

Walls/roof	**Insulation**	**Wall thickness (inches)**			
		4	**6**	**9**	**14**
Bare	Absent	3.90	3.40	3.03	2.43
Opaque walls/roof	5 mm	1.80	1.63	1.48	1.21
	10 mm	1.30	1.17	1.05	0.86
	15 mm	1.02	0.92	0.82	0.68
	20 mm	0.85	0.77	0.68	0.57
Wall/roof clad with TIM	5 mm	2.32	2.13	1.98	1.65
	10 mm	1.85	1.69	1.55	1.30
	15 mm	1.55	1.42	1.29	1.09
	20 mm	1.34	1.23	1.11	0.94

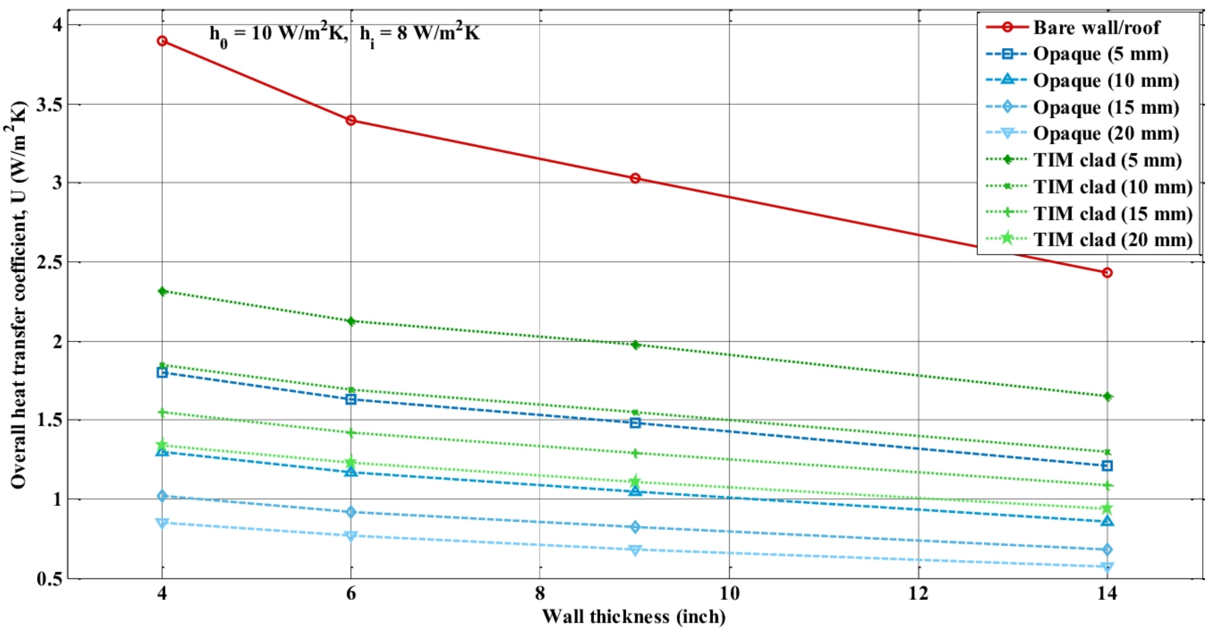

Figure 1: Variation of U with respect to L

From Fig. 1, we predicted that 20 mm TIM consistently gives the lowest U value for all wall thickness and we know that lower U value reflects minimum heat transfer and better thermal performance. Therefore, a TIM thickness of 20 mm provides the optimum thermal performance, yielding the minimum overall heat transfer coefficient across all wall

Received: December 11, 2025

International Journal of Applied Mathematics
Volume 38 No. 12s, 2025
ISSN: 1311-1728 (printed version); ISSN: 1314-8060 (on-line version)

thickness and is therefore recommended for energy-efficient passive solar building design.

To determine optimum values of design parameters for insulation devices which are applicable for building applications, Lalude and Buchberg [13] in 1971 determined optimum values of design parameters for opaque rectangular honeycombs as well as the design for a honeycomb-based, porous-bed solar air heater. In 1975, Buchberg and Edward[14] investigated the design of cylindrical glass honeycombs to minimize the cost of energy collected. Further in 1976, Hollands[15] presented the theoretical performance characteristics of a honeycomb device. Charters and Guthrie in 1982[16] have experimentally investigated the performance of a flat plate collector with a slatted convection suppression device made of thin glass. Subsequently, it was the subject of several experimental and analytical investigations related to their conductive, convective and radiative characteristics.

5 Determination of insulation characteristics for cell configuration

Combined conductive and convective heat-loss coefficient across transparent honeycomb and slat devices is given by

$$h_c = \frac{1}{L}\left[\frac{Nu\,K_a + K_w A_e}{1 + A_e}\right] \tag{6}$$

(K_a, A_a) and (K_w, A_w) are the thermal conductivities and areas of air and side wall media respectively. A_e is the relative influence of wall conduction compared to air conduction given by

$$A_e = \frac{A_w}{A_a} = \begin{cases} \dfrac{\delta(\delta + 2d)}{d^2}, & \text{for honeycomb device,} \\ \dfrac{\delta}{d}, & \text{for slat device.} \end{cases} \tag{7}$$

Total heat loss from the absorber plane includes convection through the cell and conduction & radiation through both cell and wall. It may be expressed as

$$q_1 = h_c(\theta_p - \theta_c) + \sigma F_{12}(\theta_p^4 - \theta_c^4) \tag{8}$$

$$F_{12} = \left(\frac{1}{F1R2} + \frac{1-\varepsilon_h}{\varepsilon_h} + \frac{1-\varepsilon_c}{\varepsilon_c}\right)^{-1} \tag{9}$$

Where $F1R2$ is the infra-red radiation geometrical shape factor for the cellular TIM. Following Smart et al. (1980), Nusselt number for a square cell honeycomb is given by

$$Nu = 1 + 0.89\cos(\beta - \pi/3)\left[\frac{R_a}{2420\,A^4}\right]^{(2.88 - 1.64\sin\beta)} \tag{10}$$

Where $R_a/A^4 < 6000$, $30^\circ < \beta < 90^\circ$ and $A > 4$. For parallel slat configurations, correlation for the range $R_a > R_c$, $0 \le \beta \le 75^\circ$, we have

$$Nu = 1 + c(R_a\cos\beta)^{1/3}\left[1 - \exp\left(-(a + b\beta)\left\{\left(\frac{R_a}{R_c}\right)^{(2.88 - 1.64\sin\beta)} - 1\right\}\right)\right] \tag{11}$$

$$R_c = \frac{A_e^2}{\cos\beta}\left[768 + \frac{1536A_e}{C} + \frac{48\varepsilon A_e N(1-S)}{1-(1-\varepsilon)S}\right] \tag{12}$$

Where $C = \frac{2K_a L}{K_w \varepsilon}$ (first dimensionless side wall conduction number), $N = \frac{4\sigma\theta_s^3 L}{K_a}$ (dimensionless radiation conduction number),

$$S = 1.0102 - \frac{1.4388}{A_e} - \frac{9.4653}{A_e^2} + \frac{31.440}{A_e^3} - \frac{27.515}{A_e^4} \tag{13}$$

$$q_2 = 5.7 + 3.8v(\theta_c - \theta_a) + \sigma\varepsilon(\theta_c^4 - \theta_a^4) \tag{14}$$

Overall heat transfer coefficient (U_L) and efficiency of heat collection (η) may be defined as

$$U_L = \frac{q_1}{(\theta_p - \theta_a)} \tag{15}$$

$$\eta = \tau(\theta, r) - \frac{q_1}{S} \tag{16}$$

Rectangular honeycomb with aspect ratio 8 is ideal to use if the tilt angle of absorber is in the range of 50° to 60°. Therefore, we have computationally investigated the values of U_L and η of honeycomb and slat devices at various tilt angle as shown in Fig. 2 and Fig. 3. Thermo physical parameters for the calculations are given by $\varepsilon = 0.9$, $v = 3\ \mathrm{m\,s^{-1}}$, $K_a = 0.0284\ \mathrm{W\,m^{-1}\,K^{-1}}$, $K_w = 0.21\ \mathrm{W\,m^{-1}\,K^{-1}}$, $\delta = 0.076 \times 10^{-3}$ m. For honeycomb ($L = 0.05$ m, $A = 6$); the azimuth angle $(r^\circ) = 0^\circ$. The azimuth angle (r°) for slat I ($L = 5$ cm, $d = 8$ mm), slat II ($L = 5$ cm, $d = 5$ mm) and slat III ($L = 5$ cm, $d = 6$ mm) have been taken 0°, 40° and 80° respectively.

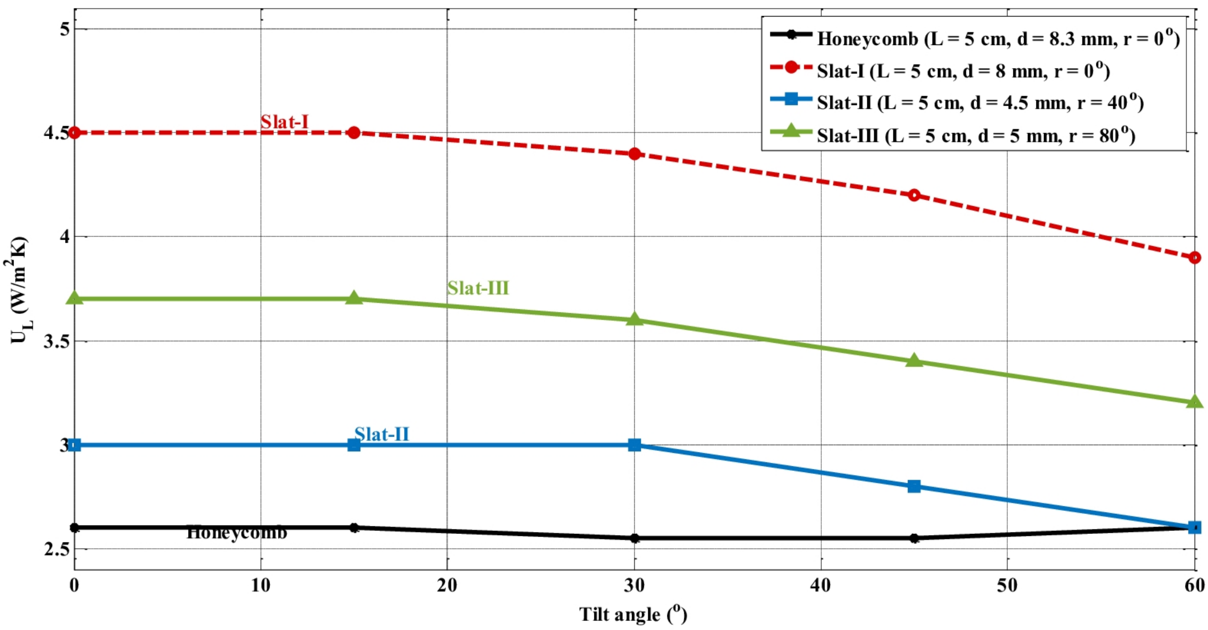

Figure 2: Heat loss across honeycomb & slat at various tilt angles

International Journal of Applied Mathematics
Volume 38 No. 12s, 2025
ISSN: 1311-1728 (printed version); ISSN: 1314-8060 (on-line version)

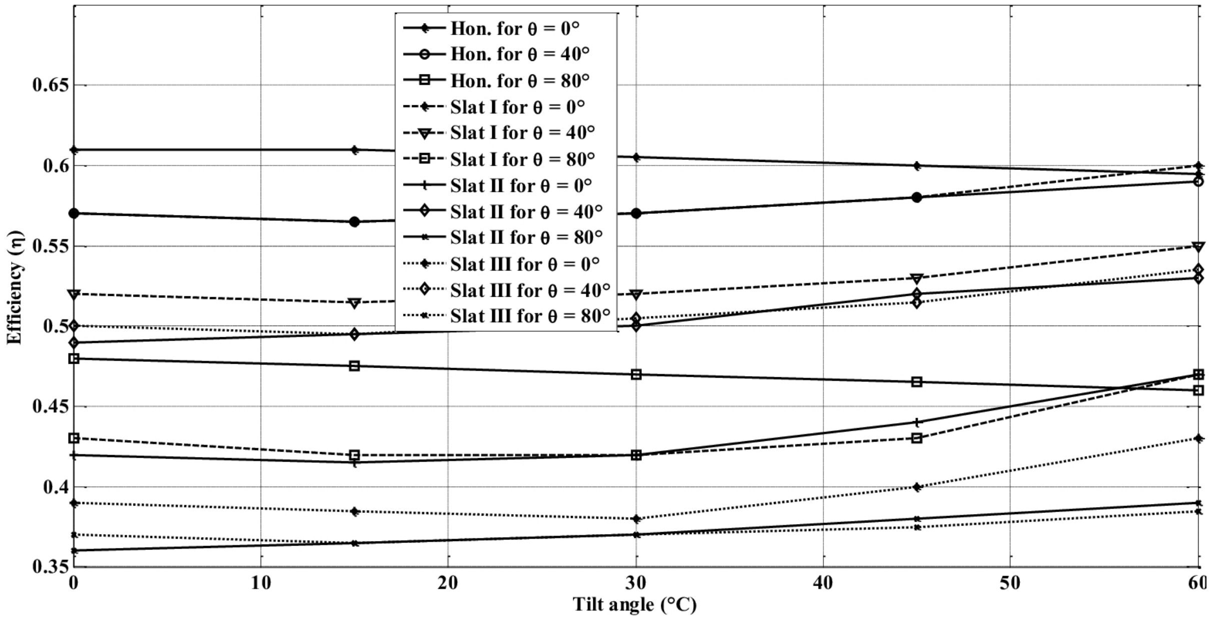

Figure 3: Efficiency of honeycomb and cell devices at various tilt angles

The computational result shows that for horizontal planes, the honeycomb exhibits superior performance, whereas a slat configuration is preferable for applications on inclined ($\beta > 30°$) planes. Following Hollands (1984)[17] and Arulanantham and Kaushika (1996)[18], a TIM device of lexan honeycomb is commercially available for building applications. The effective transmittance–absorptance product $(\alpha\tau)_{\text{eff}}$ and heat loss coefficient U_L values for the TIM cover systems involving lexan honeycomb are summarized in Table 7.

Table 7: Variation of U_L and $(\alpha\tau)_{\text{eff}}$ with depth of honeycomb

Honeycomb depth L (m)	**Aspect ratio ($A = L/d$)**	**U_L ($\mathbf{W\,m^{-2}\,K^{-1}}$)**	**$(\alpha\tau)_{\text{eff}}$ (black absorber)**
0.05	10	2.0	0.75
0.10	20	1.5	0.69
0.15	30	1.0	0.65

6 Thermal performance study of transparently insulated building

A solar thermal simulation model of a building using transparent insulation has been developed. The model can be used to investigate the steady-state as well as dynamic thermal performance of the building using TIM cover on its walls/roof. Computations have been carried out to evaluate and optimize the engineering parameters of the TIM cover and other components in a non-air-conditioned building. The objective is to examine the load level of heat flux entering the building in order to minimize the required capacity and hence reduce the capital cost of the associated building. Following Balcomb (1977)[19], Givoni (1979)[20], Kaushika (1988)[21], and Athienitis and Ramadan (1999)[22], better energy efficiency can be achieved if TIM becomes an integral part of the architectural and structural details. Numerical computations have been performed for the building parameters under consideration, which enable the assessment of

International Journal of Applied Mathematics
Volume 38 No. 12s, 2025
ISSN: 1311-1728 (printed version); ISSN: 1314-8060 (on-line version)

the influence of different components on the thermal performance of the building. Following https://power.larc.nasa.gov, the average irradiance on bare and insulated south walls for different climatic zones (Leh, Bareilly, and Hyderabad) on the 15th day of every month of 2025 has been presented in Table 8.

Table 8: Average irradiance (W m^{-2} h^{-1}) on bare and insulated south wall on 15th day of every month of 2025

Month	Leh					Bareilly					Hyderabad				
	Bare wall	5 mm	10 mm	15 mm	20 mm	Bare wall	5 mm	10 mm	15 mm	20 mm	Bare wall	5 mm	10 mm	15 mm	20 mm
January	240.6	220.4	212.1	206.3	201.8	180.5	165.2	158.6	154.1	150.3	260.5	240.8	232.9	227.2	222.9
February	300.2	275.1	265.4	258.6	253.4	220.8	202.3	194.7	189.6	185.4	310.7	286.4	276.9	270.1	265.0
March	420.8	387.6	374.2	364.5	357.2	310.6	285.4	274.8	267.2	261.5	420.3	389.5	377.1	368.2	361.5
April	560.9	517.4	499.8	486.9	477.2	420.9	388.7	375.5	366.1	359.2	520.8	482.6	467.3	456.1	447.6
May	650.5	601.2	581.6	567.1	556.3	510.4	472.8	457.6	446.3	438.1	580.9	537.4	520.2	507.4	497.8
June	680.7	629.4	608.7	593.2	581.6	540.7	500.2	483.9	471.6	462.4	560.4	519.2	502.7	490.4	481.1
July	620.3	574.8	556.6	543.1	532.9	480.2	445.6	431.9	421.7	414.2	490.2	454.1	439.7	429.0	421.0
August	590.8	548.2	531.1	518.5	509.0	450.6	418.9	406.2	396.8	389.9	470.6	436.4	422.8	412.7	405.1
September	520.6	482.4	467.1	455.8	447.3	400.3	371.8	360.5	352.1	345.9	440.8	408.9	396.2	386.8	379.7
October	410.7	380.9	369.1	360.4	353.9	320.4	297.6	288.4	281.6	276.6	380.5	353.1	342.2	334.1	328.1
November	300.9	279.2	270.4	264.0	259.1	230.7	214.2	207.5	202.6	198.9	300.6	278.9	270.1	263.7	258.9
December	250.4	229.6	221.1	215.2	210.8	190.8	175.4	169.1	164.6	161.2	270.4	250.1	242.0	236.2	231.8

The thickness of each wall has been considered of 9 inch for computational work. The computed values of average solar irradiance on south wall (Table 8) decrease consistently with increasing insulation thickness from 5 mm to 20 mm for all months and locations. In Leh, the highest irradiance occurs during the summer months (May–June), and insulation effectively reduces the incident energy on the wall surface. Similar trends are observed in Bareilly and Hyderabad, where insulated walls significantly limit solar energy absorption compared to bare walls, with 20 mm insulation providing the maximum reduction throughout the year.

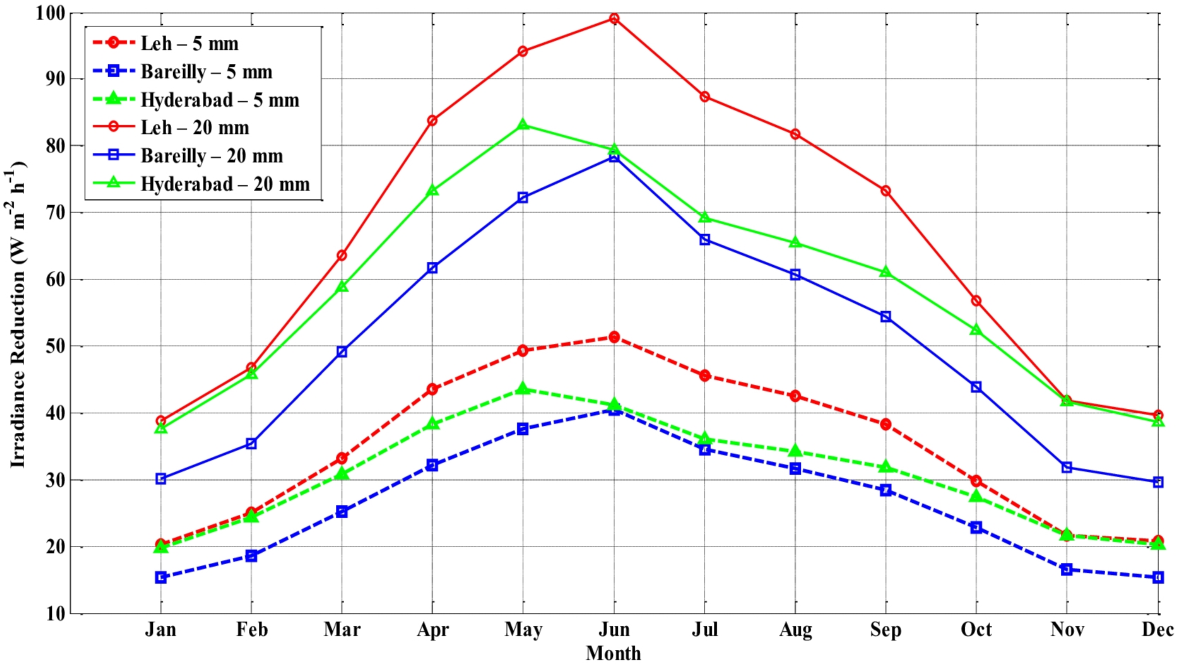

Figure 4: Irradiance reduction by using insulation on 9 inches south wall

Received: December 11, 2025

International Journal of Applied Mathematics
Volume 38 No. 12s, 2025
ISSN: 1311-1728 (printed version); ISSN: 1314-8060 (on-line version)

Fig. 4 shows that applying insulation on the 9-inch south wall leads to a clear reduction in solar irradiance compared to the bare wall condition. The irradiance reduction increases progressively with insulation thickness, with 20 mm insulation providing the maximum reduction throughout the year. This trend confirms that thicker insulation is more effective in limiting solar energy penetration through the south wall, especially during the high-irradiance summer months.

7 Effect of insulation on heat flux

This study examines the role of insulation in three cities, Leh, Bareilly and Hyderabad, which represent hot-dry with cool winters, composite and warm-humid climatic conditions, respectively. Despite high technical potential, insulation adoption in India faces barriers such as higher upfront costs, limited awareness, and weak enforcement of energy conservation measures. Therefore, insulation can significantly reduce operational energy use at peak demand. The average heat flux on the bare wall with insulation effect is presented in Table 9, which shows that insulation on the south wall substantially reduces the magnitude of average heat flux compared to the bare wall in all months.

Table 9: Average heat flux (W/m^2) on bare and insulated south wall (9″) on 15th day of every month of 2025

Month	Leh					Bareilly					Hyderabad				
	Bare wall	5 mm	10 mm	15 mm	20 mm	Bare wall	5 mm	10 mm	15 mm	20 mm	Bare wall	5 mm	10 mm	15 mm	20 mm
January	-6.85	-2.02	-1.17	-0.82	-0.62	-2.45	-0.72	-0.42	-0.30	-0.22	-1.25	-0.38	-0.22	-0.15	-0.11
February	-5.95	-1.76	-1.02	-0.72	-0.54	-1.65	-0.49	-0.29	-0.21	-0.16	-0.85	-0.26	-0.15	-0.11	-0.08
March	-3.25	-0.96	-0.56	-0.39	-0.29	0.85	0.25	0.15	0.11	0.08	1.95	0.58	0.34	0.24	0.18
April	0.45	0.13	0.08	0.06	0.04	3.95	1.17	0.68	0.48	0.36	4.65	1.38	0.80	0.56	0.42
May	4.85	1.43	0.83	0.58	0.44	7.85	2.32	1.35	0.95	0.71	7.85	2.32	1.35	0.95	0.71
June	7.95	2.35	1.36	0.96	0.72	10.25	3.03	1.76	1.24	0.93	9.45	2.79	1.62	1.14	0.85
July	6.85	2.02	1.17	0.82	0.62	8.95	2.64	1.53	1.08	0.81	8.95	2.64	1.53	1.08	0.81
August	5.95	1.76	1.02	0.72	0.54	7.65	2.26	1.31	0.92	0.69	8.15	2.41	1.40	0.99	0.74
September	3.25	0.96	0.56	0.39	0.29	5.25	1.55	0.90	0.63	0.47	6.35	1.88	1.09	0.77	0.58
October	-0.65	-0.19	-0.11	-0.08	-0.06	2.35	0.69	0.40	0.28	0.21	3.25	0.96	0.56	0.39	0.29
November	-3.85	-1.14	-0.66	-0.47	-0.35	-0.95	-0.28	-0.17	-0.12	-0.09	0.85	0.25	0.15	0.10	0.08
December	-6.25	-1.85	-1.07	-0.75	-0.56	-2.15	-0.63	-0.37	-0.26	-0.19	-0.95	-0.28	-0.16	-0.11	-0.08

Computational results show that heat flux decreasing progressively as insulation thickness increases from 5 mm to 20 mm. In Leh, insulation is most effective in winter months by significantly reducing heat loss, while also limiting summer heat gain. In Bareilly and Hyderabad, insulation markedly reduces summer heat gain, with 20 mm insulation providing the best thermal performance throughout the year.

Received: December 11, 2025

International Journal of Applied Mathematics
Volume 38 No. 12s, 2025
ISSN: 1311-1728 (printed version); ISSN: 1314-8060 (on-line version)

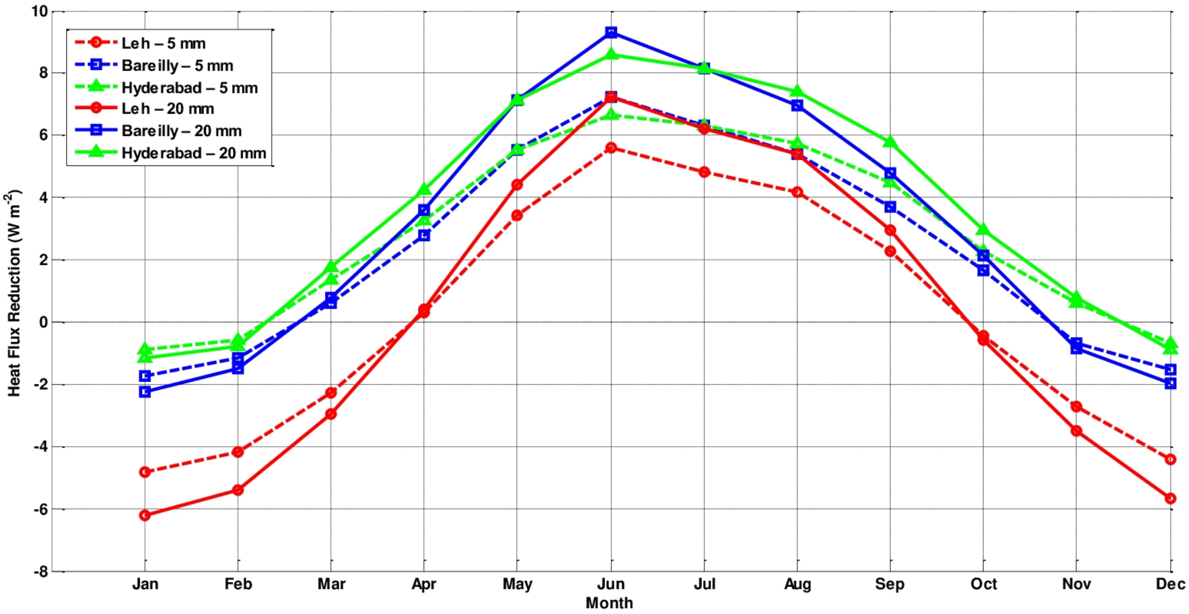

Figure 5: Heat flux (W/m^2) reduction by using insulation on 9 inches south wall

The results show that insulation on the 9-inch south wall effectively reduces heat flux in all climates, with 20 mm insulation consistently performing better than 5 mm. In Leh, insulation significantly reduces winter heat loss and limits summer heat gain, while in Bareilly it provides balanced reduction of both winter losses and summer gains. In Hyderabad, heat-flux reduction is mainly positive throughout the year, indicating high effectiveness of insulation in controlling excessive heat gain in warm climates.

8 Thermal load evaluation in a building

The thermal load formulation of a building is based on the lumped heat balance approach originally proposed by Rao and Kaushika (1984)[23], in which the indoor air temperature variation is governed by heat transfer through walls, roof, windows, ventilation, ground, and internal heat sources. When air is exchanged between inside and outside (ventilation or infiltration), heat is carried with it. Following ASHRAE Handbook–Fundamentals (2017)[24], the net thermal load of a building may be expressed as

$$Q_{\text{total}} = Q_{\text{cond}} + Q_{\text{vent}} \tag{17}$$

Where, Q_{cond} is the heat gained or lost through the building envelope such as walls, roof, windows and doors given by

$$Q_{\text{cond}} = \text{Heat entering the room} - \text{heat absorbed or removed} \tag{18}$$

Where, heat entering the room $= Q_{wl} + Q_r + Q_{wd} = Q_{wr} + Q_{wd}$ and heat absorbed or removed $= Q_f + Q_g$. The periodic conductive heat transfer through external walls is given by

$$Q_{wl} = \sum_{n=1}^{4} U_{wl}^{(n)} A_{wl}^{(n)} \left(\theta_{\text{out}} - \theta_{\text{in}}\right) \tag{19}$$

Received: December 11, 2025

International Journal of Applied Mathematics
Volume 38 No. 12s, 2025
ISSN: 1311-1728 (printed version); ISSN: 1314-8060 (on-line version)

The conductive heat transfer through roof is given by

$$Q_r = U_r A_r \left(\theta_{\text{out}} - \theta_{\text{in}}\right) \tag{20}$$

Heat transfer through window and doors includes solar heat gain and convective heat transfer given by

$$Q_{wd} = (\alpha\tau)_{\text{eff}} A_{wd} I(t) + h_{wd} A_{wd} \left(\theta_{\text{out}} - \theta_{\text{in}}\right) \tag{21}$$

The heat absorbed by furnishings known as heat storage effect of furnishings may be expressed as

$$Q_f = h_f A_f \left(\theta_{\text{in}} - \theta_{\text{out}}\right) \tag{22}$$

The heat transfer between the floor and the ground is given by

$$Q_g = h_g A_g \left(\theta_{\text{in}} - \theta_0\right) \tag{23}$$

Final combined expression may be written as

$$\begin{aligned} Q_{\text{cond}} = &\sum_{n=1}^{4} U_{wl}^{(n)} A_{wl}^{(n)} \left(\theta_{\text{out}} - \theta_{\text{in}}\right) + U_r A_r \left(\theta_{\text{out}} - \theta_{\text{in}}\right) \\ &+ (\alpha\tau)_{\text{eff}} A_{wd} I(t) + h_{wd} A_{wd} \left(\theta_{\text{out}} - \theta_{\text{in}}\right) - h_f A_f \left(\theta_{\text{in}} - \theta_{\text{out}}\right) \\ &- h_g A_g \left(\theta_{\text{in}} - \theta_0\right) \end{aligned} \tag{24}$$

Let us take steady-state assumptions for a single room in a building (wall, roof, floor, window, doors) and expressing each term in U–A–ΔT form, the effective overall heat transfer coefficient may be expressed as

$$U_{\text{eff}} = \frac{\sum_{n=1}^{4} U_{wl}^{(n)} A_{wl}^{(n)} + U_r A_r + U_{wd} A_{wd}}{A_{\text{total}}} \tag{25}$$

Where,

$$A_{\text{total}} = \sum A_{wl}^{(n)} + A_r + A_{wd}, \quad U_{wd} = (\alpha\tau)_{\text{eff}} I(t) + h_{wd},$$

thermal storage of furnishings has been neglected ($Q_f \approx 0$) and ground heat transfer has been neglected or included in U. Substituting the values of U_{eff} and A_{total} in Eq. (24), we get

$$Q_{\text{cond}} = U_{\text{eff}} \times A_{\text{total}} \times \left(\theta_{\text{out}} - \theta_{\text{in}}\right) \tag{26}$$

Following Duffie and Beckman (2013), ventilation load represents the heat gained or lost due to infiltration, natural ventilation and mechanical ventilation given by

$$Q_{\text{vent}} = Q_h - Q_v = Q_h - h_v \left(\theta_{\text{out}} - \theta_{\text{in}}\right) A_v \tag{27}$$

Where, heater effect $Q_h(t)$ may be expressed as

$$Q_h(t) = \begin{cases} q, & 0 \le t \le t_1 \\ 0, & t_1 \le t \le t_2 \\ q, & t_2 \le t \le 24 \end{cases} \tag{28}$$

Where t_1, t_2 represent the instance of switching off/on of heat source. Taking $Q_h(t) = 0$, we get

$$h_v A_v = \rho_{\text{air}} \dot{V}(t) C_p = \dot{m} C_p \tag{29}$$

Received: December 11, 2025

$$Q_{\text{vent}} = \dot{m} C_p \left(\theta_{\text{out}} - \theta_{\text{in}} \right) \tag{30}$$

Where, $\dot{V}$ is volumetric flow rate of air which lies between (0.01–0.1) m^3/s, C_p is specific heat of air, $\dot{m}$ is mass flow rate of incoming air and $\theta_{\text{out}} - \theta_{\text{in}}$ is temperature difference. Positive values indicate outside air increases cooling/heating load and negative values indicate outside air helps reduce load (e.g., cooler night air). It shows the overall heating/cooling requirement for maintaining indoor comfort.

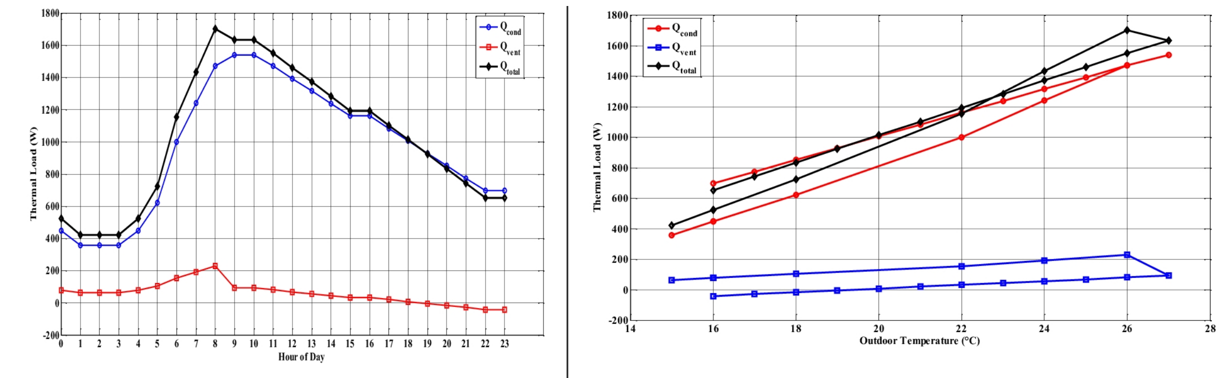

(a) Hourly thermal load

(b) Thermal load vs outdoor temperature

Figure 6: Periodic thermal load of a room on 15^{th} Nov. 2025 at Bareilly

Data of periodic thermal load of a room with above said dimensions for 15th November 2025 has been taken from the website https://www.meteostat.net and https://www.ncei.noaa.gov. The hourly thermal load shows a clear diurnal pattern, with lower values during night and early morning hours and a peak during the afternoon due to increased outdoor temperature. A strong positive correlation is observed between thermal load and outdoor temperature, indicating that higher ambient temperatures lead to greater heat gain through the building envelope. This confirms that outdoor temperature is the dominant factor governing the periodic thermal load of the room at Bareilly on 15 November 2025.

9 Effect on thermal load with variable wind speed and door opening period

Let us assume that door of the room has been opened at a gap of 2 hours in each opening on dated 15-11-2025 in Bareilly. Opening period and wind speed in each case has been taken according to Table 10. We have investigated the above three cases on 15 November

Table 10: Case study for door opening and wind speed

	Case I	**Case II**	**Case III**
Door opening	10 sec	10 sec	30 sec
Wind speed	1 m/s	2 m/s	1 m/s

at Bareilly with above defined dimensions. Effect on thermal load by opening/closing of the door with assumed wind speed has been represented by Fig. 7.

International Journal of Applied Mathematics
Volume 38 No. 12s, 2025
ISSN: 1311-1728 (printed version); ISSN: 1314-8060 (on-line version)

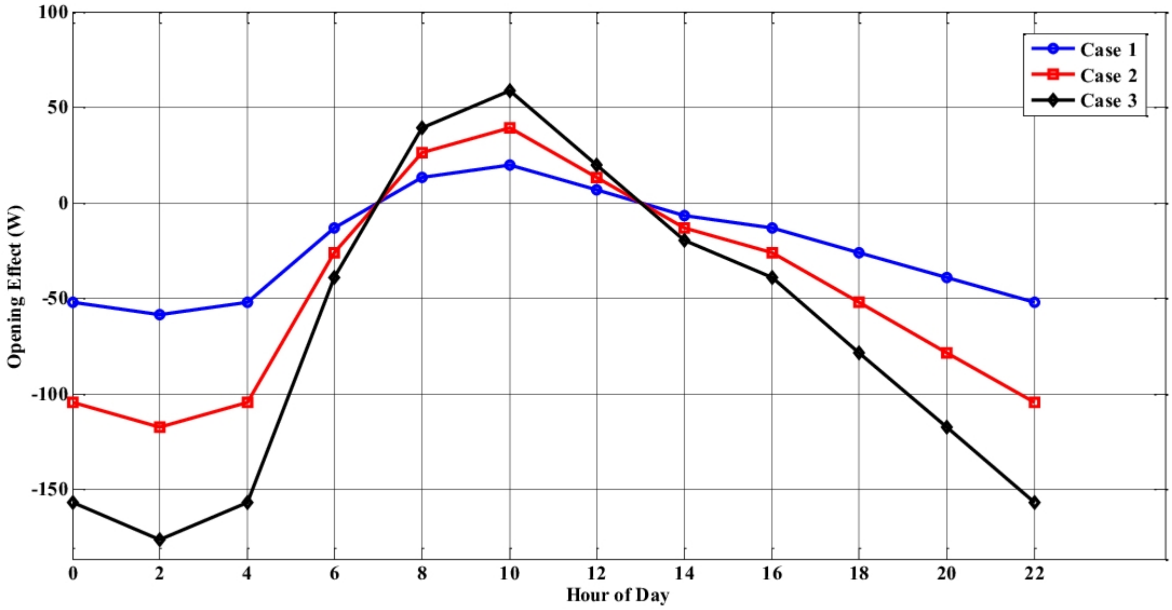

Figure 7: Effect on thermal load by opening/closing of the door

In Case 1, door opening under low wind speed (1.0 m/s) causes a moderate reduction in thermal load during night and early morning hours (up to 59 W), while the effect is minimal around early morning. During daytime, it slightly increases the thermal load due to warm air ingress, whereas in the evening and night hours it again helps in reducing the load.

In Case 2, increasing the wind speed to 2.0 m/s significantly amplifies the effect of door opening, leading to large reductions in thermal load during night and early morning hours (up to about 118 W). However, during daytime hours, door opening results in noticeable heat gains due to the entry of warmer outdoor air, while substantial reductions are again observed in the evening and night periods.

In Case 3, increasing the door opening duration to 30 s at a wind speed of 1.0 m/s results in the largest variation in thermal load, with substantial reductions during night and early morning hours (up to about 176 W). During daytime, door opening leads to higher heat gains due to warm air ingress, while significant cooling effects are again observed during evening and night hours.

10 Effect of insulation in thermal load of a building

The net thermal load of a proposed room with insulation of 5, 10, 15, and 20 mm on south wall at Leh and Bareilly on 15-11-2025 has been analyzed with the help of sources https://www.meteostat.net and https://www.ncei.noaa.gov.

Table 11: Thermal load of a room with insulation effect on south wall on 15–11–2025

Time	θ_{out} (°C)	Leh: Thermal load (W)				θ_{out} (°C)	Bareilly: Thermal load (W)			
		5 mm	10 mm	15 mm	20 mm		5 mm	10 mm	15 mm	20 mm
0	-8	-4120.35	-4053.72	-4004.35	-3966.42	16	-1643.27	-1616.70	-1597.02	-1581.87

Continued on next page

Received: December 11, 2025

International Journal of Applied Mathematics
Volume 38 No. 12s, 2025
ISSN: 1311-1728 (printed version); ISSN: 1314-8060 (on-line version)

Time	θ_{out} (°C)	Leh: Thermal load (W)				θ_{out} (°C)	Bareilly: Thermal load (W)			
		5 mm	10 mm	15 mm	20 mm		5 mm	10 mm	15 mm	20 mm
1	-9	-4325.76	-4255.80	-4203.96	-4164.16	15	-1848.68	-1818.78	-1796.65	-1779.60
2	-9	-4325.76	-4255.80	-4203.96	-4164.16	15	-1848.68	-1818.78	-1796.65	-1779.60
3	-10	-4531.17	-4457.89	-4403.57	-4361.89	15	-1848.68	-1818.78	-1796.65	-1779.60
4	-10	-4531.17	-4457.89	-4403.57	-4361.89	16	-1643.27	-1616.70	-1597.02	-1581.87
5	-9	-4325.76	-4255.80	-4203.96	-4164.16	18	-1232.45	-1212.52	-1197.77	-1186.40
6	-7	-3914.94	-3851.63	-3804.74	-3768.68	22	-410.82	-404.17	-399.26	-395.47
7	-5	-3504.12	-3447.46	-3405.52	-3373.21	24	0	0	0	0
8	-3	-3093.29	-3043.29	-3006.30	-2977.74	26	410.82	404.17	399.26	395.47
9	-1	-2682.47	-2639.12	-2607.09	-2582.27	27	616.23	606.26	598.88	593.20
10	0	-2477.06	-2437.38	-2408.48	-2386.16	27	616.23	606.26	598.88	593.20
11	1	-2271.65	-2235.64	-2209.87	-2189.96	26	410.82	404.17	399.26	395.47
12	2	-2066.23	-2033.90	-2010.26	-1991.76	25	205.41	202.09	199.63	197.73
13	1	-2271.65	-2235.64	-2209.87	-2189.96	24	0	0	0	0
14	0	-2477.06	-2437.38	-2408.48	-2386.16	23	-205.41	-202.09	-199.63	-197.73
15	-1	-2682.47	-2639.12	-2607.09	-2582.27	22	-410.82	-404.17	-399.26	-395.47
16	-2	-2887.88	-2840.86	-2805.70	-2778.38	22	-410.82	-404.17	-399.26	-395.47
17	-4	-3298.71	-3245.03	-3205.91	-3175.77	21	-616.23	-606.26	-598.88	-593.20
18	-6	-3709.53	-3649.20	-3604.13	-3569.16	20	-821.63	-808.35	-798.51	-790.93
19	-7	-3914.94	-3851.63	-3804.74	-3768.68	19	-1027.04	-1010.44	-998.14	-988.67
20	-8	-4120.35	-4053.72	-4004.35	-3966.42	18	-1232.45	-1212.52	-1197.77	-1186.40
21	-9	-4325.76	-4255.80	-4203.96	-4164.16	17	-1437.86	-1414.61	-1397.39	-1384.13
22	-9	-4325.76	-4255.80	-4203.96	-4164.16	16	-1643.27	-1616.70	-1597.02	-1581.87
23	-8	-4120.35	-4053.72	-4004.35	-3966.42	16	-1643.27	-1616.70	-1597.02	-1581.87

On 15 November 2025, the hourly thermal load of the south wall shows a clear climatic contrast between Leh and Bareilly. In Leh, the thermal load remains negative throughout the day, indicating continuous heat loss and a dominant heating requirement; however, increasing insulation thickness from 5 mm to 20 mm consistently reduces the magnitude of this heat loss, with thicker insulation yielding the lowest (least negative) thermal loads as represented in Table 10. In Bareilly, the thermal load varies from negative values during night and early morning hours to zero or positive values around midday, reflecting a transition from heating demand to slight cooling requirement; here also, higher insulation thickness effectively moderates both heat losses and gains. Overall, insulation thicknesses of 15–20 mm are most effective in stabilizing the hourly thermal load, with the impact of insulation being more pronounced under the colder climatic conditions of Leh.

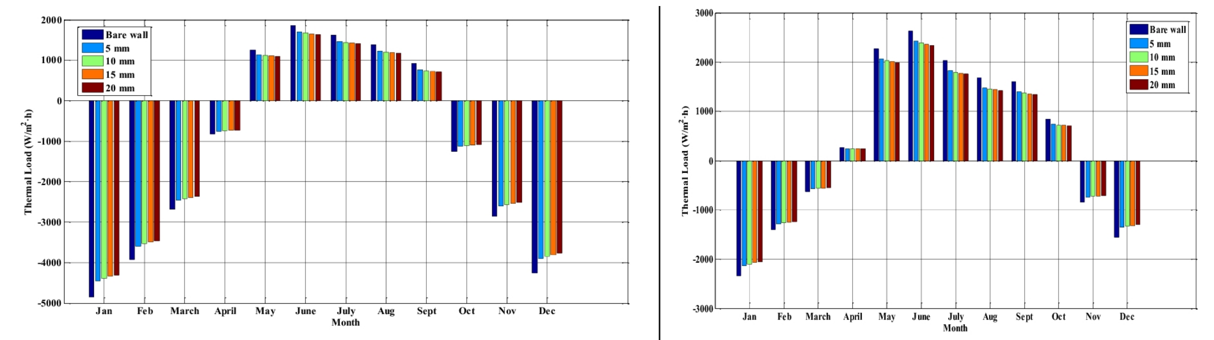

(a) Leh (b) Bareilly

Figure 8: Monthly thermal load with insulation effect on south wall

In Fig. 8 Leh and Bareilly highlight a clear climatic contrast in south-wall thermal performance. Leh exhibits predominantly negative thermal loads throughout most of the year, indicating a strong heating demand, with only short summer periods showing positive values, whereas Bareilly shows negative thermal loads in winter months and positive thermal loads during summer, reflecting a seasonal shift from heating to cooling demand. In both locations, the application of insulation consistently reduces the magnitude of thermal load compared to bare walls, and the reduction becomes more pronounced as insulation thickness increases from 5 mm to 20 mm. Overall, the 20 mm insulation provides the maximum improvement in thermal performance in both climates, with a more significant impact observed in the colder climatic conditions of Leh.

Conclusion

This study demonstrates that the application of opaque insulation and transparent honeycomb insulation materials significantly enhances the thermal performance of building envelopes across diverse climatic conditions. The results confirm that increasing insulation thickness consistently reduces overall heat transfer coefficients, heat flux, and thermal load, with a thickness of 20 mm identified as optimal for all climates considered. While opaque insulation provides maximum thermal resistance, TIM-clad walls offer a balanced trade-off between heat loss reduction and solar transmission, making them suitable for passive solar applications. Overall, transparent honeycomb insulation shows strong potential for reducing building energy demand and supporting energy-efficient building design.

Acknowledgement

The authors wish to thanks to **Uttar Pradesh Government** to sanction Grant for the project entitled “Energy Economic and Planning for Sustainable Development in Uttar Pradesh” through letter “No-**24/2023/681/ Sattar-4-2023-002-4(59)/2022 Dated 28-03-2023”**.

References

[1] Y. A. Cengel and A. J. Ghajar. *Heat and Mass Transfer.* McGraw-Hill, 5 edition, 2015.

[2] ASHRAE. *Handbook of Fundamentals.* ASHRAE, Atlanta, 2021.

[3] D. B. Crawley et al. Energyplus: Energy simulation program. *Energy and Buildings*, 33(4):319–331, 2001.

[4] TRNSYS. *A Transient System Simulation Program.* Solar Energy Laboratory, University of Wisconsin–Madison, 2017.

[5] J. Clarke. *Energy Simulation in Building Design.* Butterworth-Heinemann, 2 edition, 2001.

[6] DesignBuilder Software Ltd. *DesignBuilder Simulation Tool*, 2021.

[7] A. Aslani et al. Bim–bem integration for building energy modelling. *Energy and Buildings*, 202:109–129, 2019.

International Journal of Applied Mathematics
Volume 38 No. 12s, 2025
ISSN: 1311-1728 (printed version); ISSN: 1314-8060 (on-line version)

[8] Y. Pan et al. Advances and challenges in building energy modelling. *Energy and Buildings*, 262, 2022.

[9] S. Attia. *Building Performance Simulation for Design and Operation.* Springer, 2018.

[10] G. N. Tiwari and R. Ghosh. *Solar Energy: Fundamentals, Design, Modelling and Applications.* Narosa, 2016.

[11] N. Zhu et al. Phase change materials for building applications. *Applied Energy*, 86:203–210, 2009.

[12] A. Khalifa and A. Abbas. Recent advances in pcms. *Energy Storage*, 4(2):1–23, 2021.

[13] H. Buchberg, O. A. Lalude, and D. K. Edwards. Performance characteristics of rectangular honeycomb solar thermal converters. *Solar Energy*, 1971.

[14] H. Buchberg and D. K. Edwards. Design consideration for solar collectors with cylindrical glass honeycombs. *Solar Energy*, 1975.

[15] K. G. T. Hollands, L. Konicek, T. E. Unny, and G. D. Raithby. Free convection heat transfer across inclined air layers. *Journal of Heat Transfer*, 1976.

[16] K. I. Guthrie and W. W. S. Charters. An evaluation of a transverse slatted flat plate collector. *Solar Energy*, 1982.

[17] K. G. T. Hollands, G. D. Raithby, F. B. Russell, and R. G. Wilkinson. Coupled radiative and conductive heat transfer across honeycomb panels and through single cells. *Journal of Heat Transfer*, 1984.

[18] M. Arulanantham and N. D. Kaushika. Coupled radiative and conductive thermal transfer across transparent honeycomb insulation materials. *Solar Energy*, 1996.

[19] J. D. Balcomb, J. C. Hedstrom, and R. D. McFarland. Simulation analysis of passive solar heated buildings: Preliminary results. *Solar Energy*, 1977.

[20] B. Givoni. *Passive Cooling of Buildings by Natural Energies.* Van Nostrand Reinhold, 1979.

[21] N. D. Kaushika. *Principles and Applications of Solar Energy.* Wiley Eastern, 1988.

[22] A. K. Athienitis and H. Ramadan. Numerical model of a building with transparent insulation. *Energy and Buildings*, 1999.

[23] S. K. Rao and N. D. Kaushika. *Energy Conversion Management.* Wiley Eastern, 1984.

[24] ASHRAE. *ASHRAE Handbook–Fundamentals.* ASHRAE, 2017.